LASER INTERFEROMETER GRAVITATIONAL WAVE OBSERVATORY
- LIGO -
CALIFORNIA INSTITUTE OF TECHNOLOGY
MASSACHUSETTS INSTITUTE OF TECHNOLOGY

Technical Note	**LIGO-T2000370–v1**	2020/07/30

Optical Refrigeration — Interim Report 1

S. Schulz
Mentors: R. Adhikari, Y. Drori, C. Wipf

California Institute of Technology
LIGO Project, MS 18-34
Pasadena, CA 91125
Phone (626) 395-2129
Fax (626) 304-9834
E-mail: info@ligo.caltech.edu

Massachusetts Institute of Technology
LIGO Project, Room NW22-295
Cambridge, MA 02139
Phone (617) 253-4824
Fax (617) 253-7014
E-mail: info@ligo.mit.edu

LIGO Hanford Observatory
Route 10, Mile Marker 2
Richland, WA 99352
Phone (509) 372-8106
Fax (509) 372-8137
E-mail: info@ligo.caltech.edu

LIGO Livingston Observatory
19100 LIGO Lane
Livingston, LA 70754
Phone (225) 686-3100
Fax (225) 686-7189
E-mail: info@ligo.caltech.edu

http://www.ligo.caltech.edu/

1 Introduction

1.1 Motivation

Gravitational waves (GWs) are ripples in spacetime which propagate at the speed of light and are caused by the acceleration of massive objects. Their existence was predicted in 1916 by Albert Einstein when he developed the general theory of relativity [1]. The Laser Interferometer Gravitational-wave Observatory (LIGO) is a national facility for GW research consisting of two interferometer observatories with a goal of observing and understanding these GWs and the events that cause them [2]. In order to detect GWs, LIGO observatories must be able to detect changes in length in their 4 km arms many orders of magnitude smaller than the radius of a proton, and the smaller changes they are able to detect, the more GW events can be observed [3]. The current observatory design, called Advanced LIGO (aLIGO) has detected many GW events since the first observation in 2015, and improvements continue to be made on that design [2]. Soon, this design will reach the limits of its detection capabilities brought about by thermodynamics and quantum mechanics. In order to continue to improve detector sensitivity, a new upgrade is planned called "Voyager LIGO" which aims to increase the observation range 4-5 times and the detected event rate by a factor of 100 [4]. Voyager would operate at 123 K and use silicon mirrors to reduce thermo-elastic noise.

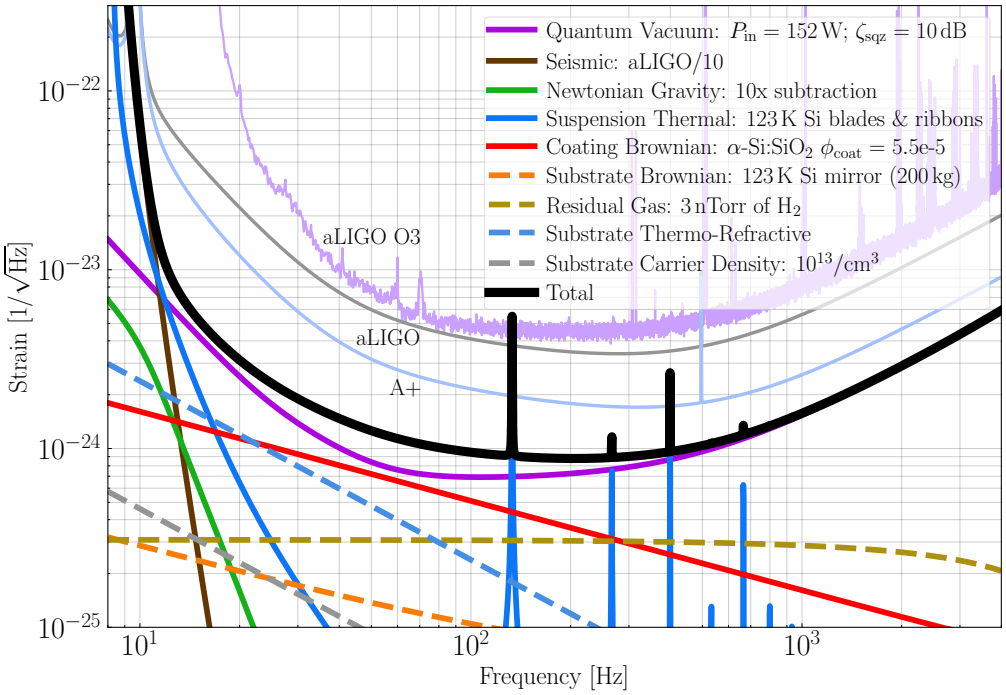

Figure 1: The target noise curve for LIGO Voyager as compared to noise curves for other LIGO designs. Figure from [4].

As can be seen in Figure 1, even for the Voyager design, the main source of noise for most detection frequencies is quantum noise, which arises due to random fluctuations in photon number travelling through the apparatus [5]. One parameter that sets a bound on quantum noise is the laser power circulating in each of the 4 km arms. Although aLIGO operates

at a power of ∼750 kW in each of its arms, any increase in that number would allow for more quantum sensitivity. Because Voyager aims to operate at cryogenic temperatures, any increase in cavity laser power must have a corresponding increase in cooling of the end test mass in order to combat heating caused by absorption. Because LIGO observatories measure only one variable, the relative length of the arms, LIGO has been able to use "squeezed vacuum" injected into the interferometer to significantly decrease quantum noise [6]. However, the effectiveness of any quantum noise reduction is still limited by losses in interferometer optics. To combat this, a phase-sensitive optomechanical amplifier (PSOMA) has been proposed, which is capable of mitigating optical losses and reducing quantum noise [7]. Like the rest of the interferometer, the optics used for PSOMA must be kept at around 123 K because the device will use the same silicon mirrors as the rest of Voyager.

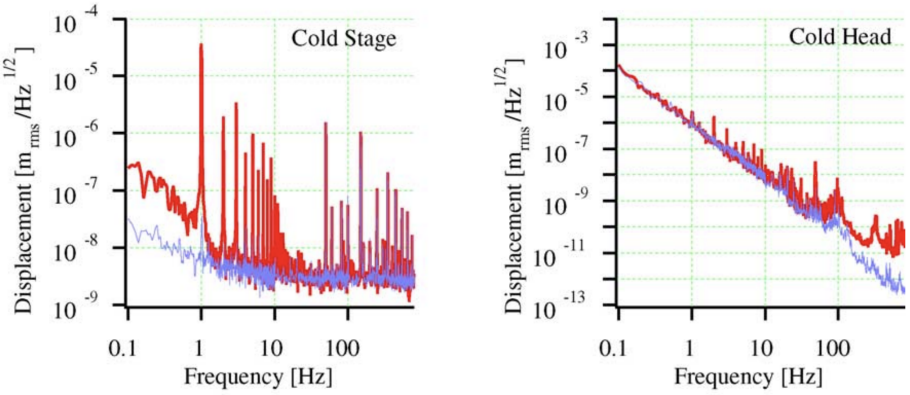

Figure 2: Vibration spectra for a 4 K pulse-tube cryocooler. The blue lines are the sensor noise while the red lines are the measured vibration in the cryocooler. The cold head and cold stage represent different parts of the cryocooler. Figure from [8].

Clearly, both of these ways of reducing quantum noise require cooling. Because any introduced vibration to the test mass would increase noise, cryocooling techniques must introduce little to no vibration to the system. Vibrations are also harmful near the test mass even if none of the vibration is transferred to it. This is because some laser light might be scattered off of the test mass onto surrounding objects before recombining with the main beam. If those objects are vibrating, a phase shift could be introduced along with fluctuations in radiation pressure, both of which would contribute to the noise [15]. Most cryocoolers cool by mechanically coupling the load to a cooling element which has some amount of vibration, which means that vibration would be introduced to the load. Figure 2 shows a vibration spectrum of a "low-vibration" cryocooler that was being looked at for other high sensitivity devices [8]. The vibration appears at some points negligible compared to the sensor noise, but the cold stage shows several peaks at harmonics of the 1 Hz fundamental and the cold head shows some measurable vibration above about 100 Hz, which is well within the detection bandwidth of LIGO. Figure 3 shows the maximum allowed displacement for the inner heat shield around the test mass. Comparing Figure 2 with Figure 3, we can clearly see that the vibrations of the cryocooler exceed those acceptable for the Voyager design. Although thermoelectric coolers can be vibration-free, they cannot operate at cryogenic temperatures and therefore are not an option. Radiative cooling can often be useful, but has strict up-

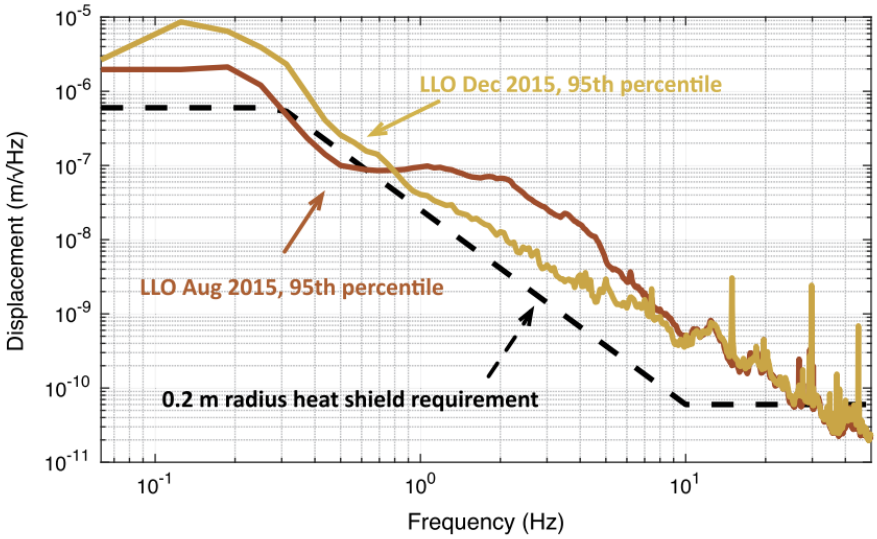

Figure 3: 95th percentile displacement spectra for LIGO Livingston and the maximum permitted displacement for the inner heat shield for the test mass. The inner heat shield is the object closest to the test mass. Figure from [15].

per limits imposed by the finite size of the optical components. One potential solution to this problem is to use a solid-state optical refrigerator to cool the interferometer, which is vibration free and can cool all the way to cryogenic temperatures.

1.2 Optical Refrigeration

The foremost method for optical refrigeration takes advantage of a quantum mechanical material phenomenon called anti-Stokes fluorescence, where the average fluorescence energy for a particular substance exceeds the average absorbed energy. To begin to understand this process, take the example a crystal doped with Yb^{3+}, the most common type of material used for optical refrigeration. Some other rare-earth (RE) ions exhibit similar behavior with only slightly different level structures, so this is a good model for all potential coolant materials [9]. When Yb^{3+} is embedded in its crystal field, its $^2F_{7/2}$ ground state and $^2F_{5/2}$ excited state manifolds split into 4 and 3 levels respectively due to a Stark shift [9], as shown on the left in Figure 4. In order to simplify the math and understanding of the process, a simpler four level model is used, as shown on the right in Figure 4. This model shows the relevant processes for optical refrigeration: pumped excitation, radiative decay, nonradiative decay, and thermalization within each manifold due to phonon absorption. For RE-doped crystals, the rethermalization rate is much faster than either decay rate, which allows the system to settle in an excited state quasi-equilibrium before decaying [9]. This is the origin of the anti-Stokes shift; some excited Yb^{3+} ions will thermalize into the $|3\rangle$ state before decaying either to the $|0\rangle$ or $|1\rangle$ state. Similarly, the ions which decay into $|0\rangle$ must thermalize into $|1\rangle$ before they can be pumped to the excited state.

If we assume the spin degeneracy of each level to be the same and apply Boltzmann statistics

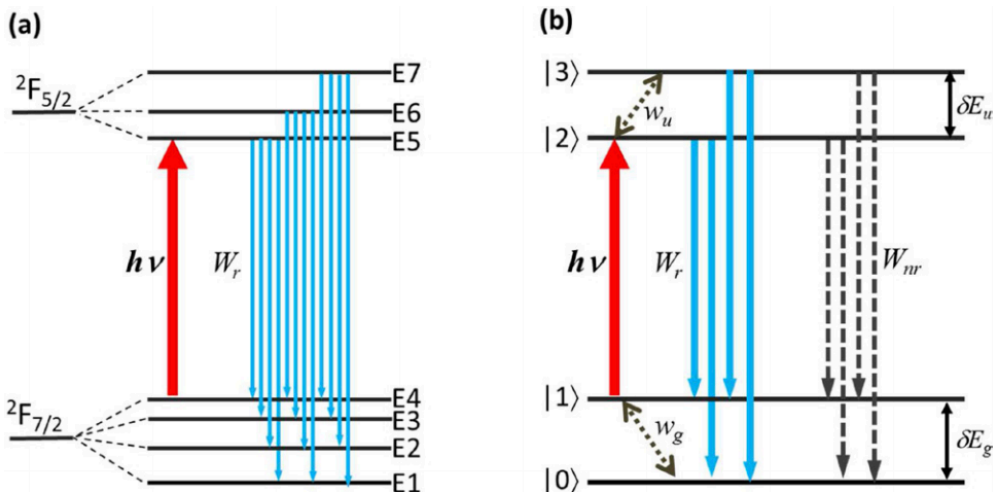

Figure 4: **(a)** The Stark-shifted level structure for Yb^{3+} showing all possible radiative decay processes, with the total rate of these processes being W_r, as well as the optical pumping at frequency ν. **(b)** A simplifed four-level model used to explain the cooling cycle for optical refrigeration, where the radiative and nonradiative decay rates are given by W_r and W_{nr} respectively. The phononic excitation rates are shown here as w_g for the ground state and w_u for the excited state. The width of the ground and excited state manifolds are given by δE_g and δE_u respectively. Figure from [9].

using the bulk temperature T of the crystal, we can arrive at expressions relating to the populations of each energy level for a system containing N_t ions, given by N_0, N_1, N_2, and N_3:

$$\frac{dN_1}{dt} = -\sigma_{12}\left(N_1 - N_2\right)\frac{I}{h\nu} + \frac{R}{2}\left(N_2 + N_3\right) - w_g\left(N_1 - N_0 e^{-\delta E_g/k_B T}\right), \tag{1}$$

$$\frac{dN_2}{dt} = \sigma_{12}\left(N_1 - N_2\right)\frac{I}{h\nu} - RN_2 + w_u\left(N_3 - N_2 e^{-\delta E_u/k_B T}\right), \tag{2}$$

$$\frac{dN_3}{dt} = -RN_3 - w_u\left(N_3 - N_2 e^{-\delta E_u/k_B T}\right), \tag{3}$$

$$N_0 + N_1 + N_2 + N_3 = N_t \tag{4}$$

where σ_{12} is the absorption cross-section for the $|1\rangle - |2\rangle$ transition, I is the irradiance of the pump laser, $R = 2\left(W_r + W_{nr}\right)$ is the total decay rate for the excited state, and k_B is the Boltzmann constant [9]. Additionally, we can arrive at an expression for the net power deposited to system by summing the absorbed power by the ions, the radiated power, and parasitically absorbed power as follows:

$$P_{net} = \sigma_{12}\left(N_1 - N_2\right)I - W_r\left[N_2\left(E_{21} + E_{20}\right) + N_3\left(E_{31} + E_{30}\right)\right] + \alpha_b I \tag{5}$$

where E_{xy} is the energy difference between $|x\rangle$ and $|y\rangle$, and α_b is the total parasitic absorption coefficient [9]. Next, we can write the absorption coefficient accounting for saturation by setting all of the time derivates equal to zero to find steady state behavior

$$\alpha = \frac{\alpha_0}{1 + I/I_s} \tag{6}$$

where

$$\alpha_0 = \sigma_{12} N_t \frac{e^{-\delta E_g/k_B T}}{1 + e^{-\delta E_g/k_B T}} \tag{7}$$

and

$$I_s = \frac{h\nu R}{\sigma_{12} Z_{gu}} \tag{8}$$

where $Z_{gu} \approx 1 + e^{-\delta E_g/k_B T}$[9]. Combining all of these, we get

$$P_{net} = \alpha I \left(1 - \eta_q \frac{h\nu_f}{h\nu}\right) + \alpha_b I, \tag{9}$$

where quantum efficiency $\eta_q = (1 + W_{nr}/W_r)^{-1}$ has been introduced and the mean fluorescence energy is given by

$$h\nu_f = h\nu + \frac{\delta E_g}{2} + \frac{\delta E_u}{1 + (1 + R/w_u)\, e^{\delta E_u/k_B T}} \text{[9]}. \tag{10}$$

P_{net}, being the net power deposited to the coolant, will be negative for a cooling system. This number as shown depends on both input light wavelength and temperature (in several places) so these parameters will have to be explored in order to optimize cooling power. The cooling power depends on several material parameters, including $R, w_{g,u}, \delta E_{g,u}, \sigma_{12}$ and α_b. For RE-doped systems, $R \ll w_{g,u}$, so differences in these two values can largely be ignored [9].

Although many of the considerations in choosing a material will pertain to particularities of the interaction between the ion and its host, one can in general decouple the properties of the two and therefore in this review the properties of several ions and several hosts will be considered separately before making a conclusion on a particular ion-host pair. The primary consideration in the choice of host and ion will be in optimizing the cooling power which can be written as $P_{cool} = -P_{net}$, with P_{net} as written in Equation 9

The properties relating to the material are the absorption coefficient α, the background absorption coefficient α_b the mean fluorescence energy $h\nu_f$ (which informs the choice of pump energy $h\nu$) and the quantum efficiency $\eta_q = (1 + W_{nr}/W_r)^{-1}$, which is given in terms of the ratio of the nonradiative decay rate W_r to the radiative decay rate W_r [9]. The model that informs the above equation does not account for phonon reabsorption, so often η_q is replaced with external quantum efficiency η_{ext}, which is a more easily measurable quantity that represents the fraction of excited ions that remove a photon from the system [17]. The absorption terms are often reorganized into an absorption efficiency, expressed as $\eta_{abs} = \alpha/(\alpha_b + \alpha)$, which represents the proportion of light absorbed that goes to exciting the coolant system. It is worth noting that α, α_b, ν_f, and η_{ext} are all temperature dependent, but the temperature dependences of α_b and η_{ext} are small and can largely be ignored. Recent findings have shown that α_b actually decreases with lower temperature, but this effect is thought to be largely dependent on the particularities of the impurities in the system [18].

Often when discussing materials, a related parameter called the cooling efficiency is used, defined as

$$\eta_c = \frac{P_{cool}}{P_{abs}}, \tag{11}$$

,

where $P_{abs} = I(\alpha+\alpha_b)$ is the total absorbed power. The cooling efficiency can also be written as

$$\eta_c = \eta_{abs}\eta_q \frac{h\nu_f}{h\nu} - 1, \tag{12}$$

where all the variables are defined as before. Here either the internal quantum efficiency η_q or the external quantum efficiency η_{ext} may be used depending on context and a positive cooling efficiency corresponds to net cooling.

Another way of writing the cooling power, in terms of the cooling efficiency η_c, is as follows:

$$P_{cool} = \eta_c P_{abs}. \tag{13}$$

This formulation often ends up being very convenient, especially when you can assume P_abs to be on the order of the incident power of the pump laser. This approximation is reasonably valid as long as the optical path is such that the beam passes through the crystal several times, and there are several strategies to ensure this condition [19]. Making this approximation, we are left with

$$P_{cool} \approx \eta_c P_{in}, \tag{14}$$

where P_{in} is the power of the pump beam. This tells us that improvements to efficiency are roughly equivalent to improvements in cooling power.

In general, to optimize cooling power and efficiency, high quantum and absorption efficiency are desired. There are also considerations relating to the energy scale of the transitions. Using lower energy transitions can lead to higher cooling power if all other parameters are kept similar. The best way to understand this is by looking at Equation 9 and assuming that there is very little parasitic absorption and the quantum efficiency is near 1, as would have to be true in any usable optical refrigerator. This gives $P_{cool} \sim \alpha I(h\nu_f - h\nu)/(h\nu)$. In general for optical coolants, the difference $h\nu_f - h\nu$ tends to be of order k_BT independent of the pump energy scale due to that difference coming from rethermalization within the manifolds [16]. This means that $P_{cool} \propto k_BT/(h\nu)$, meaning that a lower energy gap could lead to higher cooling power as long as parasitic absorption and nonradiative decay are still able to be minimized. Additionally, the fluorescence energy informs the type of laser that can be used to excite the system, as the high power lasers that would be required for certain energy gaps are sometimes either unavailable or impractically expensive. Another consideration is how closely the level structure resembles the ideal one used to derive Equation 9. If there

are effects present that that model ignores, such as other excited states, the power could depart from that expected from Equation 9.

A final consideration is the minimum achievable temperature T_m of a material, which is the temperature at which a coolant no longer cools (P_{cool} goes to zero). Put plainly, if a material does not cool at the relevant temperatures for LIGO interferometer equipment, it will not be able to be used in a cryocooler. For the mirrors to be used for LIGO Voyager, that temperature is 123 K. T_m depends on the same material properties as the cooling power (η_{ext}, α, α_b, and ν_f) all of which are temperature dependent to varying extents as discussed before.

For optical cooling to be useful for LIGO, a high-power refrigerator capable of cooling the relevant systems would have to be designed. Considerations will have to be made about the coolant material, the thermal coupling to the load, and the housing for such a system. To start, a prototype optical refrigerator must be designed to explore how the technique might be useful and demonstrate a proof of concept of cooling a load.

2 Progress

2.1 Identification of coolant Ion

Thus far, five potential RE ions have been identified as candidates for use in optical refrigeration. As shown in Figure 5, these are the tripositive ions of elements 66-70: Dy^{3+}, Ho^{3+}, Er^{3+}, Tm^{3+}, and Yb^{3+} [12]. Of these, all but Dy^{3+} have been used as dopants in successful optical refrigeration experiments.

2.1.1 Ytterbium

Yb^{3+} is far and away the most widely used coolant ion for optical refrigeration. The first demonstration of optical cooling [20], the first system cooled to below 100 K [21], and the first solid-state optical cryocooler [10] all used Yb^{3+}-doped coolants. Yb^{3+} has several advantages over most other potential dopants. The Stark-shifted level structure of the ion very closely resembles the ideal four-level model used to derive Equation 9 in that there are no nearby excited states above the $F_{5/2}$ one (Figure 5). This means that there is no possibility of excited state absorption, which can introduce some nonradiative emission processes and add unwanted thermal energy to the coolant [12]. The relevant transition for Yb^3+ also has a relatively high absorption cross-section as compared to other candidate ions, which both increases absorption efficiency and makes Yb^3+ more forgiving to some impurities that may cause background absorption [12]. That transition is at a relatively high energy of $\sim$1 µm which has a couple of benefits. First, that energy is much higher than the phonon energies present in most of the possible hosts, which makes nonradiative processes like multiphonon relaxation much less likely, allowing for very high quantum efficiency [12]. Additionally, there exist many commercially available and affordable lasers at that energy with sufficient power to achieve high power cooling which becomes important in practical implementation of an optical refrigerator.

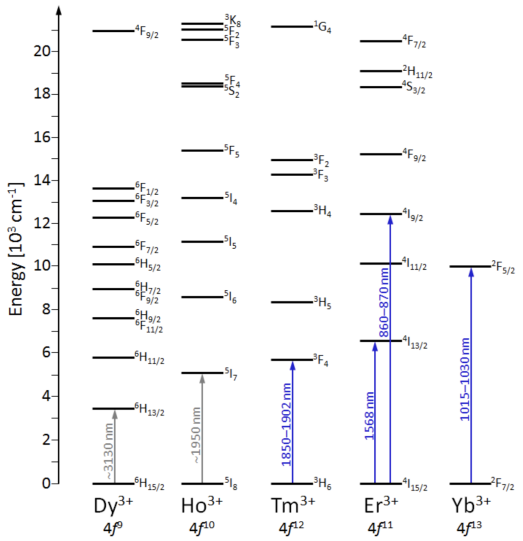

Figure 5: The ions that have been proposed for use in optical coolants and the relevant transitions. Blue lines indicate that the transition has been successfully used to cool. Note that since the publication of this figure, net cooling has been shown in a Ho^{3+}-doped system [14]. Figure from [12].

Yb-doped hosts offer an extensive amount of proven success that makes them attractive to be used for a demonstration of optical refrigeration.

It is also worth noting here that recently hosts doped a small amount of Tm^3+ in addition to Yb^3+ have shown efficiency improvements over those doped with only Yb^3+ [24]. The intentional introduction of a Tm impurity has been shown to significantly reduce background absorption, allowing for higher efficiencies. However, this research is new and these crystals are not readily available at the moment.

2.1.2 Thulium

Thulium was first used in an experiment that demonstrated net cooling in 2000 [22]. The relevant cooling transition for thulium is in the ∼1.8-2 µm range. As stated before, this could allow for higher cooling power and efficiency than for the ∼1 µm range seen in Ytterbium-doped systems. However, Tm-doped systems have to date only been able to cool 19 K from room temperature [23]. This is partly due to a difficulty in scaling the amount of dopant while keeping the purity low with current crystal growth techniques. Additionally, Tm-doped hosts have lower absorption cross-section. Both of these facts lower the absorption efficiency and therefore limit the minimum achievable temperature significantly. Additionally, because the energy gap is much lower than that of Yb^3+, nonradiative decay through multiphonon relaxation is much more likely because these decay rates increase exponentially with decreasing energy gap, although that effect can mostly be minimized with the proper choice of host [22]. Additionally, high power lasers in this energy range are less common, which reduces the practicality of these materials.

2.1.3 Erbium

Erbium is different than the other potential coolant ions in that it has several transitions with appropriate level structures for anti-Stokes fluorescence cooling. Net cooling using the $^4I_{15/2}$-$^4I_{9/2}$ transition was demonstrated first in 2006 [25]. One advantage of this transition is that there exist readily available lasers in the required energy range. Cooling using the $^4I_{15/2}$-$^4I_{13/2}$ transition was first realized in 2009 [26]. However, both of these transitions have faced limitations due to the complications introduced by the presence of other nearby excited states, and presently there is no real outlook for their potential use in cryocoolers. Another approach involved pumping the $^4I_{15/2}$-$^4S_{3/2}$ transition, which allows for some population of the $^2H_{11/2}$ manifold in addition to the normal thermalization within manifolds [27]. However, this has only been shown to work at high (>300 K) temperatures and is therefore impractical for our purposes.

2.1.4 Holmium

Although no holmium-doped solid showed bulk cooling until much later than the other materials mentioned here, recent studies have shown great promise for their use in optical cryocoolers. The first successful net cooling was demonstrated in 2016 [14]. Ho^{3+}-doped hosts have several advantages over the other hosts that take advantage of lower energy gaps like Tm. One is that the absorption cross-section at high energy is relatively high, allowing for a high absorption coefficient [28]. Also, the excited state manifold is narrow, which makes the mean fluorescence energy less temperature dependent [28]. Another important fact is that the minimum achievable temperature of ∼130 K for Ho^{3+}-doped YLF (to be discussed more later) is expected to be achieved by pumping with ∼2070 nm light, where there are readily available high power fiber lasers suitable for pumping in an optical refrigerator. The final, and potentially biggest, advantage of using a Ho-doped coolant for our purposes is that the fluorescence would mostly be invisible to the silicon test mass or PSOMA mirrors. This means that if some fluorescent light were to leak out of the coolant enclosure, it would deposit almost no heat into the mirror. However, one potential disadvantage of fluorescence in this wavelength range is that light at exactly the wavelength of the interferometer laser may couple to that beam and introduce noise. Research into Ho-doped materials is still very new, and successful implementation of a cryocooler using a Ho-doped sample would depend on some advances in quantum efficiency and doping percentage of these materials so that they may cool efficiently as low as 123 K (Figure 6).

2.2 Identification of coolant Host

2.2.1 Fluorozirconate Glasses

A large portion of early optical refrigeration experiments used fluorozirconate glasses like ZBLAN and ZBLANP as hosts for Yb ions. These hosts were attractive because they were extensively used in the telecommunications industry and thus very high purity samples were available. The lowest temperature achieved in a fluorozirconate host was 208 K in 2005 [29]. Since then, optical refrigeration research has focused on crystals hosts rather than glass hosts. Crystals hosts are capable of much higher absorption as well as higher conductivity,

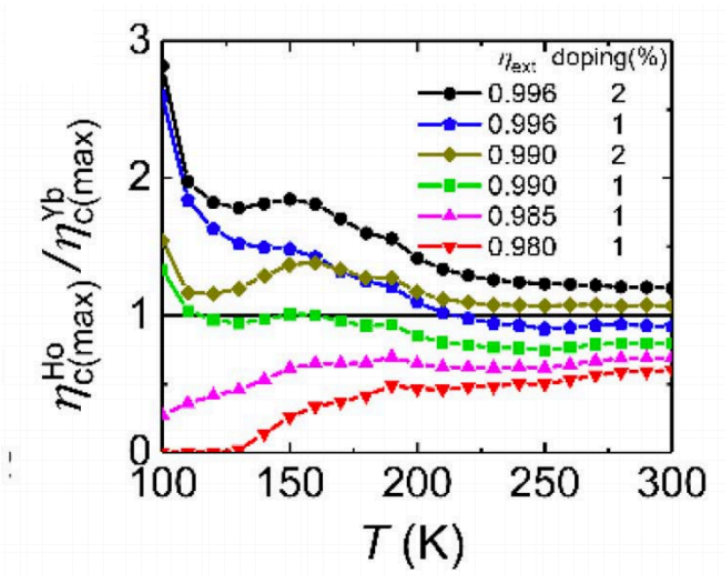

Figure 6: A graph showing the ratio of expected maximum cooling efficiencies at different temperatures of Ho:YLF coolant to the optimal efficiencies found in Yb:YLF. We can see that Ho:YLF has the potential for significant efficiency improvements at low temperature, especially with improvements to quantum efficiency. Figure from [28]

which becomes important in any cryocooling application [12].

2.2.2 BYF

One of the first candidate crystal hosts used for optical refrigeration was BaY_2F_8 (BYF). BYF has many attractive properties including a very low phonon energy which suppresses nonradiative decay, high thermal conductivity, and reasonably low broadening of the ground and excited-state manifolds [12]. However, research into increasing the doping concentration of these crystals has not made much progress, so other crystals such as YLF have taken over as better candidates for solid-state cryocoolers.

2.2.3 YLF

Although some other crystals have been used as hosts in successful cooling experiments, recent experiments for both Yb and Ho-doped hosts (as well as Tm) have revolved around $YLiF_4$—known as YLF—as a host. The physical properties of YLF offer several advantages over competing hosts. One is that it has a relatively low maximum phonon energy at around $450\,cm^{-1}$, making nonradiative multiphonon relaxation exceedingly unlikely and allowing for a high quantum efficiency [12]. Additionally, Yb:YLF has been shown to have a relatively high absorption cross-section at cooling wavelengths. The most important advantages of YLF, however, come from the chemistry involved in the crystal growing process. For materials with sufficiently high quantum efficiency, maximizing absorption and minimizing background absorption become the most important things. In terms of the material, that is achieved by maximizing the doping percent and minimizing the presence of impurities. Both

of these have been able to be achieved in Yb:YLF through years of crystal growth research [19]. For Ho:YLF this research is still new, so it is hard to evaluate the doping limits of such crystals.

2.3 Conclusions

Here we have determined that using Yb:YLF as a coolant for our optical refrigeration demonstration will be the best course of action. Although Ho:YLF shows promise and potential for higher cooling power at cryogenic temperatures as well as fluorescence that may be easier to shield from the test masses, the research into such coolants is not progressed enough for it to be a reliable choice for a demonstration. Currently we are in contact with a couple crystal manufacturers in search of a suitable crystal to be used as a coolant.

2.4 Design of an Optical Refrigeration Demonstration

Now that a coolant material has been identified, there are some high level considerations that must be made in designing an optical refrigeration demonstration. To date, optical cryocooling has been demonstrated both in with a load mostly transparent to the fluorescence from the coolant crystal and in an arbitrary load with no particular beneficial properties relating to its absorption spectrum [30] [10]. The reason the absorption properties get special consideration is that the absorption of fluorescence by the load has the potential to overwhelm any cooling in the system as will be shown here later. For our own demonstration, we have considered the potential advantages of each type of optical cryocooler. A schematic for each cryocooler is shown in Figure 7. Both designs have some common elements beyond the choice of coolant crystal, designed to minimize the various heat loads that may be on the system. They both are in a vacuum and use low thermal conductivity supports to isolate the system from any nearby conductive heat sources. Both demonstrations would make use of low-emissivity material in the support structure to minimize radiative load on the system. They both would make use of a multipass optical path so that absorption may be maximized in the coolant crystal. The difference lies in how they deal with the issue of fluorescence absorption by the load, which leads each demonstration to be able to simulate slightly different applications of optical refrigeration. The transparent load design can ignore this problem due to the low absorption coefficient in the relevant frequency band. The arbitrary load design makes use of a "thermal link," which is used to shield the load from fluorescent light. Other strategies such as putting a highly reflective mirror at the link-cold finger interface may additionally be useful in achieving that same goal.

The major advantage of the arbitrary load design is inherent in the name: it could theoretically be scaled to cool any load that can be effectively thermally linked to it. This could lead to broad applicability of such a design especially in the near future to be used for sensors or other small instruments. Due to the current limits on cooling power at cryogenic temperatures, these applications are probably the most likely until the technique develops further. Using such a design would also allow for tackling complicated engineering problems, such as optimizing the shape of the thermal link. The transparent load design would be effective in simulating a cryocooler that might be particularly useful for cooling large silicon mirrors to be used in an interferometer. The lack of thermal link should allow for higher cooling powers

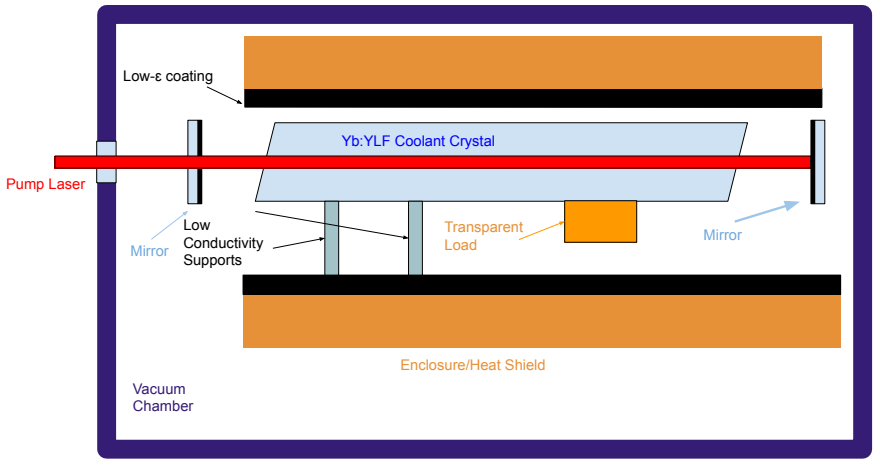

(a) Demonstration with transparent load

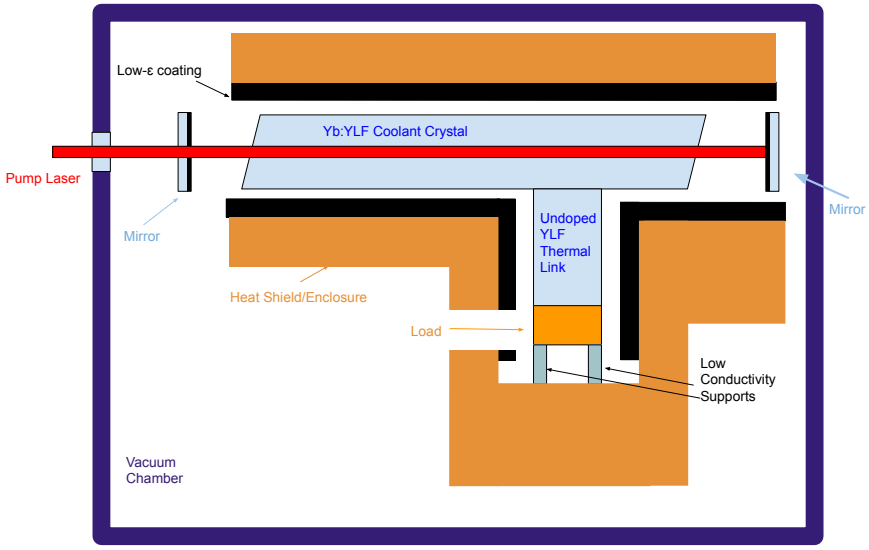

(b) Demonstration with arbitrary load

Figure 7: The two possible designs for an optical refrigeration experiment. Note that they are largely the same with the main difference being the use of an undoped YLF thermal link in the design with an arbitrary load.

both due to lower radiative loads and a shorter conductive heat path. As mentioned above, silicon is largely transparent to the fluorescence of an Ho-doped host. Using a Yb-doped host with a load that is transparent to its fluorescence may allow us to effectively simulate a silicon mirror cooled by an Ho-doped host. If such a system is able to produce high cooling powers, it may end up being an effective solution to cool the large test mass mirrors at LIGO. Additionally, modeling how the radiation pressure of the fluorescence on the reflective dielectric coatings of the mirrors might create noise in the interferometer would be useful in determining the applicability of this technique.

We have decided to begin to pursue both designs, but with an emphasis on the arbitrary load design due to its short term applicability.

2.5 Determination of Temperature Dynamics

In order to determine how an optical refrigeration demonstration will evolve over time, a mathematical model for the temperature evolution of such a system had to be created. The simplest way to do this is my assuming that temperature dispersion within each body (coolant crystal, thermal link, load) happens relatively quickly. This allows us to model the system as either a two-body or three-body system, depending on whether a thermal link is present. As of this moment, modeling has been done for the two-body system, which will be shown as follows. The equations governing temperature evolution in the coolant (at temperature T_c) and load (at temperature T_l) can be written as

$$C_c \frac{dT_c}{dt} = -P_{net} + P_{rad,c}(T_c) + P_{cond}(T_c, T_l), \tag{15}$$

$$C_l \frac{dT_l}{dt} = -P_{cond}(T_c, T_l) + P_{rad,l}(T_l) + \beta P_{rad} + P_{load}, \tag{16}$$

where C_c and C_l are the the heat capacities of the crystal (c) or load (l), P_{net} is from Equation 9, $P_{rad,c}$ and $P_{rad,l}$ are the radiative head load from the chamber walls on each body, P_{cond} is the power of the conductive heat transfer from the load to the crystal, $P_{rad} = \eta_{ext} P_{abs}$ is the power of the fluorescence radiated from the coolant crystal, β is the proportion of that fluorescence that is absorbed by the load, and P_{load} is any other external heat load on the system. Expressions for each of these power terms can be found in already published papers that demonstrate optical cryocooling [10] [30]. Note that the conductive heat load due to the supports of the crystal-load system is not included here, but that load has been found to be negligible compared to the radiative load [30]. These equations can be solved numerically to find temperature evolution for each body. These equations could also be extended to solve the three-body case, but that calculation is still in progress.

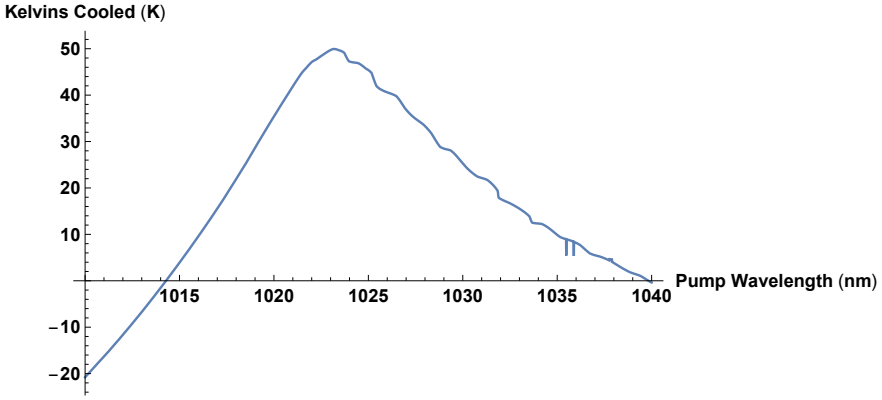

Figure 8: Amount cooled vs. pump wavelength for the load in a two-body optical refrigeration demonstration pumped by a 2 W laser. The most cooling is achieved by pumping at 1023 nm.

For the two-body case, we evaluated these equations for a Yb:YLF crystal cooling a 10 g copper load with no external power on the load. The cooling power was calculated using existing absorption data for Yb:YLF [31]. The main desired results of these calculations were

to find how the cooling dynamics would depend on the pump wavelength, the pump laser power, and how well shielded the load is from the coolant's fluorescence. The wavelength dependence on the minimum temperature is demonstrated in figure 8. This has indicated to us that at the lower laser powers that we would likely use for a demonstration, it is likely best to pump the system at 1023 nm. Figure 10 demonstrates the necessity of minimizing the absorbed radiation by the load. This makes sense because the coolant crystal fluoresces at a much higher power than the cooling power. This informs the fact that we either must choose a transparent load or shield the load from circulating fluorescence. Figure 9 tells us that for the goal of simply creating a demonstration, a lower power ($\sim$1 W) pump laser would be sufficient to cool by a few kelvin as is desired.

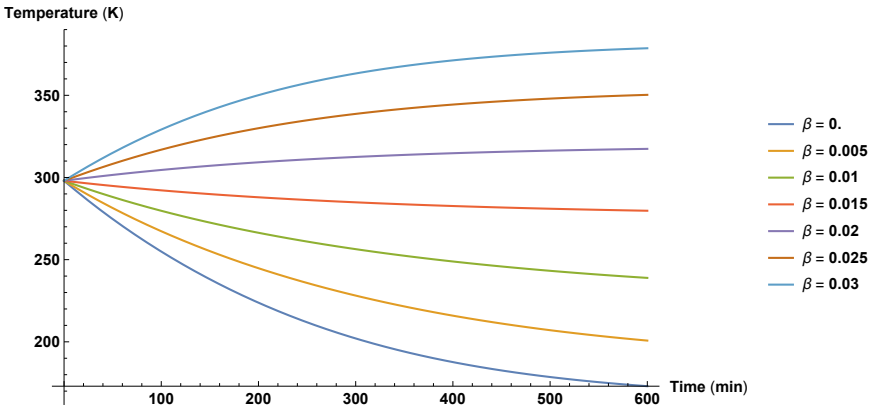

Figure 9: Temperature evolution for the load in a two-body optical refrigeration demonstration with varying β, the proportion of fluorescence absorbed by the load, pumped by a 2 W laser at 1023 nm. It is clear here that minimizing β is crucial for any net cooling to occur.

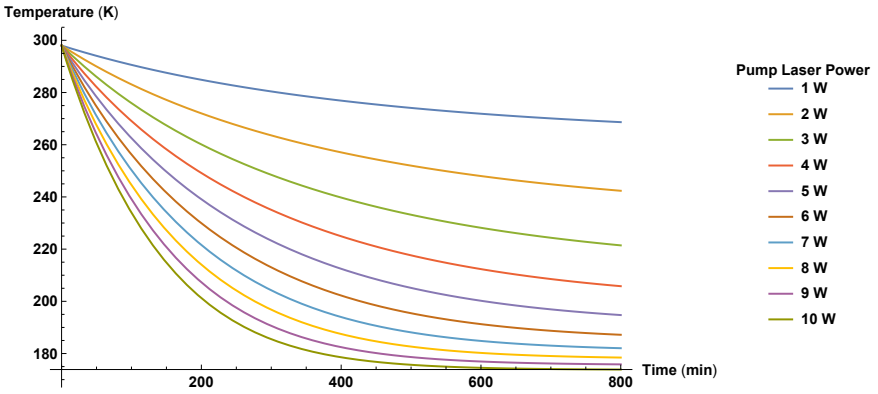

Figure 10: Temperature evolution for the load in a two-body optical refrigeration demonstration with varying pump power for the input 1023 nm laser, assuming a value of .009 for β. This shows us that a system that will cool at high pump power will likely also cool at lower pump power, albeit to a much higher final temperature and much slower.

3 Cooling of PSOMA Mirrors

Due to limitations of lab access surrounding the ongoing pandemic, we have shifted some of the main goals of the project from designing a demonstration of optical refrigeration to looking at applications for how an optical refrigerator might be implemented in LIGO. One of those applications is cooling the mirrors in the proposed phase-sensitive optomechanical amplifier for LIGO Voyager. The PSOMA mirrors, like the rest of those used in Voyager, will be made primarily out of pure silicon to leverage its special thermal expansion properties. Importantly, the design of PSOMA favors mirrors that are light so that they may be susceptible to radiation pressure. This limits the efficacy of cooling these mirrors radiatively because the total surface area is limited by the both the mass of the silicon and the necessity of a large enough mirror face to reflect the incident beam. The existence of this limit could make the an optical refrigerator useful to add additional cooling. The need for cooling comes from the absorption by the mirror coatings of a very small amount of the circulating power. The more power circulating, the less noise in the amplifier, so more cooling leads to less total noise [7].

3.1 The Limits of Radiative Cooling for PSOMA

As mentioned above, the small size of the PSOMA mirrors puts a limit on the degree to which they can be cooled radiatively. Here we will try to establish an approximate value for that upper limit. To do so, we use the Stefan-Boltzmann law to find the radiated power P for each mirror surface,

$$P = A\sigma\varepsilon T^4 \tag{17}$$

where A is the surface area of that surface, ε is the emissivity of that surface, σ is the Stefan-Boltzmann constant ($\sim 5.67 \times 10^{-8}\,\mathrm{W\,m^{-2}\,K^{-4}}$), and T is the temperature, which for PSOMA will be 123 K. If we assume that the mirror surface will be circular with a diameter about 1.5 times the beam diameter (10 mm) and that the mass of the mirror will be 30 g, we can find the exact dimensions of a cylindrical mirror with those properties. By using ε values of 0.5 and 0.9 for the dielectric coating and silicon surfaces respectively [4], we can find the power radiated by each surface and sum them to find the total radiated power. A simple calculation finds a radiated power of ~ 45 mW at 123 K. Any real implementation of radiative cooling would by necessity have a cooling power lower than that figure due to the radiative load placed on the mirror by its environment. Assuming 1 ppm absorption by the mirror, this would allow for a power circulating in the cavity of up to ~ 45 kW. For a 10 g mirror with the same properties otherwise, a maximum of ~ 17 mW could be cooled radiatively, allowing for a circulating power of ~ 17 kW. For both mirrors, the cooling power is $\sim 1.4\,\mathrm{kW\,g^{-1}}$

3.2 Prospects of Optical Cooling for PSOMA

To explore the possibility of using optical refrigeration for PSOMA mirrors, we can use the same mathematical framework established to design the optical refrigeration demonstration. For an actual implementation for LIGO, the best possible setup would be used, so those are the parameters we will use here. Unlike for a demonstration, the clear choice for dopant ion

is holmium, because the silicon mirrors will have very low absorption across the fluorescence band of Ho^{3+} ($\sim 2\,\mu m$). The minimum achievable temperature for any holmium-doped crystals that appear in currently published papers is not low enough to cool at 123 K, so we must consider some development in the quantum efficiency or doping concentration in those crystals [28]. However, work has been done in investigating how improved holmium-doped crystals might preform in an optical refrigerator, so the theoretical specification improvements of those crystals will be used here [28]. Because the load will be largely transparent to the crystal's fluorescence, there will be no need to use a thermal link or shield the load, so the crystal can be adhered directly to the mirror with the optical path of the pump laser running perpendicular to the normal of the mirror surface. We use existing spectroscopy, background absorption, and external quantum efficiency measurements as a basis for these calculations before making some modifications for particular theoretical crystals [28]. In particular we will start with a real crystal with the 1% doping concentration and 0.980 η_{ext}, as well as hypothetical crystals with $\eta_{ext} = .985$, 0.990 and 0.996 and crystals with 2% doping concentration, which would double the absorption coefficient [28]. Using these parameters, we find that the highest cooling performance at 123 K would be when the crystal is pumped at $\sim 2065\,nm$. Lasers operating at 2070 nm have been produced which output nearly 100 W, so a slightly conservative 80 W of pumping will be used in this calculation [32]. The most successful optical cooling experiments to date have been performed in an astigmatic Herriott cell to allow for a many-pass configuration [33]. The best performing Herriott cells used for this application have given over 150 round trips, so here we will use 120 round trips with a mirror reflectivity of 0.99 [33]. We additionally assume that the addition of the coolant crystal will have minimal effect on the radiative load on the system. Just like for the radiative cooling, we will assume an absorption of 1 ppm by the coating of the PSOMA mirror. Calculated values for offset power, defined to be the amount of additional power that could circulate in the cavity without heating the mirror when cooled by the crystal at 123 K are plotted against mass in Figure **??**.

References

[1] https://www.ligo.caltech.edu/page/what-are-gw

[2] https://www.ligo.caltech.edu/page/about

[3] https://www.ligo.caltech.edu/page/ligos-ifo

[4] R.X. Adhikari et al., *A Cryogenic Silicon Interferometer for Gravitational-wave Detection*; arXiv:2001.11173 (2020).

[5] The LIGO Scientific Collaboration et al., *Advanced LIGO*; Class. Quantum Grav. **32** 074001 (2015).

[6] https://www.ligo.caltech.edu/mit/page/research-development;

[7] Y. Bai et al., *A phase-sensitive optomechanical amplifier for quantum noise reduction in laser interferometers*; arXiv:1909.02264 (2019).

[8] T. Tomaru et al., *Vibration analysis of cryocoolers*; Cryogenics **34** 309-317 (2004).

[9] D.V. Seletskiy et al., *Laser cooling in solids: advances and prospects*; Rep. Prog. Phys. **79** 096401 (2016).

[10] M.P. Hehlen et al., *First demonstration of an all-solid-state optical cryocooler*; Light: Science & Applications **7** 15 (2018).

[11] S. Bigotta et al., *Single fluoride crystals as materials for laser cooling applications*; Proc. SPIE **6461**, Laser Cooling of Solids (2007).

[12] M.P. Hehlen et al., *Solid-state Optical Refrigeration*; Handbook on the Physics and Chemistry of Rare-Earths **46** (2014).

[13] N.J. Condon et al., *Optical cooling in Er3+:KPb2Cl5*; Optics Express **17** 7 (2009).

[14] S. Rostami et al., *Optical refrigeration of Tm:YLF and Ho:YLF crystals* Proc. SPIE **9765**; Optical and Electronic Cooling of Solids (2016).

[15] B. Shapiro et al, *Cryogenically cooled ultra low vibration silicon mirrors for gravitational wave observatories*; Cryogenics **81** 83 (2017).

[16] C.W. Hoyt et al, *Observation of Anti-Stokes Fluorescence Cooling in Thulium-Doped Glass*; Phys. Rev. Lett. **85** 17 (2000).

[17] D.V. Seletskiy et al., *Local laser cooling of Yb:YLF to 110 K*; Optics Express **19**, (2011).

[18] A. Volpi et al., *Optical refrigeration: the role of parasitic absorption at cryogenic temperatures*; Optics Express **27**, (2019).

[19] D.V. Seletskiy et al., *Cryogenic optical refrigeration*; Adv. Opt. Photon. **4**, (2012).

[20] R. I. Epstein et al., *Observation of laser-induced fluorescent cooling of a solid*; Nature **377**, (1995).

[21] S.D. Melgaard et al., *Solid-state optical refrigeration to sub-100 Kelvin regime*; Scientific Reports **6**, (2016)

[22] C.W. Hoyt et al., *Observation of Anti-Stokes Fluorescence Cooling in Thulium-Doped Glass*; Phys. Rev. Lett **85** (2000).

[23] C.W. Hoyt et al., *Advances in laser cooling of thulium-doped glass*; J. Opt. Soc. Am. **20**, (2003).

[24] G. Cittadino et al., *First demonstration of optical refrigeration efficiency greater than 4% at room temperature*; Optics Express **28**, (2020).

[25] J. Fernandez et al., *Anti-Stokes Laser Cooling in Bulk Erbium-Doped Materials*; Phys. Rev. Lett. **97**, (2006).

[26] N.J. Condon et al., *Optical cooling in Er3+:KPb2Cl5*; Optics Express **17**, (2009).

[27] G.Z. Sui et al., *Laser cooling with optical temperature sensing in Er3+-doped tellurite-germanate glasses*; Appl. Phys. B. **110**, (2013).

[28] S. Rostami et al., *Observation of optical refrigeration in a holmium-doped crystal*; Photonics Research **7**, (2019).

[29] J. Thiede et al., *Cooling to 208 K by optical refrigeration*; Appl. Phys. Lett., **86**, (2005).

[30] D.V. Seletskiy et al., *Laser cooling of a semiconductor load to 165 K* ; Optics Express **18**, (2010).

[31] D.V. Seletskiy et al., *Precise Determination of Minimum Achievable Temperature for Solid-State Optical Refrigeration*; arXiv:1203.5967 (2012).

[32] K. Yin et al., *High-power all-fiber wavelength-tunable thulium doped fiber laser at 2 μm*; Optics Express **22**, (2014).

[33] A. Gragossian et al., *Astigmatic Herriott cell for optical refrigeration*; Optical Engineering **56**, (2017).